Ultrafast dynamics of the dipole moment reversal in a polar organic monolayer

Natalia García Rey (iD), and Heike Arnolds (iD)

View Online   Export Citation   CrossMark

ARTICLES YOU MAY BE INTERESTED IN

Submit Today

The Journal of Chemical Physics

The Emerging Investigators Special Collection and Awards
Recognizing the excellent work of early career researchers!

AIP Publishing

Ultrafast dynamics of the dipole moment reversal in a polar organic monolayer

Natalia García Rey[1,a] and Heike Arnolds[2]

AFFILIATIONS

[1] Institute of Physical Chemistry, Westfälische Wilhelms-Universität Münster Corrensstraße 28/30, 48149 Münster, Germany

[2] Surface Science Research Center, Department of Chemistry, University of Liverpool, Oxford Road, Liverpool L69 3BX, United Kingdom

Note: This article is part of the Special Topic "Nonlinear Spectroscopy and Interfacial Structure and Dynamics" in J. Chem. Phys.
[a] Author to whom correspondence should be addressed: ngarciarey@uni-muenster.de

ABSTRACT

Pyridine layers on Cu(110) possess a strong electric field due to the large dipole of adsorbed pyridine. This electric field is visible as an enhanced sum frequency response from both the copper surface electrons and the aromatic C–H stretch of pyridine via a third order susceptibility. In response to a visible pump pulse, both surface electron and C–H stretch sum frequency signals are reduced on a subpicosecond time scale. In addition, the relative phase between the two signals changes over a few hundred femtoseconds, which indicates a change in the electronic structure of the adsorbate. We explain the transients as a consequence of the previously observed pyridine dipole field reversal when the pump pulse excites electrons into the pyridine π^* orbital. The pyridine anions in the pyridine layer cause a large-scale structural change which alters the pyridine-copper bond, reflected in the altered sum frequency response.

Published under license by AIP Publishing. https://doi.org/10.1063/1.5066551

INTRODUCTION

Photoinduced electron transfer coupled to molecular motion at metal-molecule interfaces controls surface photochemistry and determines device performance in molecular electronics or nanoplasmonics.[1–4] The strength of nonadiabatic coupling between the electronic degrees of freedom and nuclear position is a key issue in many surface dynamic processes such as adsorption, diffusion, reaction, and desorption.[5] It can be probed with femtosecond laser pump-probe spectroscopy, where the pump pulse creates a hot electron distribution for around 1 ps and a time-delayed probe pulse monitors the ensuing adsorbate nuclear motion through vibrational or electronic spectroscopy.

An established vibrational probe is broadband infrared-visible sum frequency generation (SFG),[6] which has uncovered coupling times between molecular vibrations and excited electrons ranging from several hundred femtoseconds to a few picoseconds for diffusion,[7] desorption,[8–10] and reaction.[11,12]

The vast majority of these pump-probe studies have been carried out on CO adsorbed at metal surfaces. The observed nonadiabatic dynamics are often attributed to anharmonic coupling between internal and external vibrational modes although some experimental and theoretical work indicates that the transients are caused by charge transfer from the hot electron bath to the CO $2\pi^*$ antibonding state.[12–15]

In order to broaden our understanding of nonadiabatic adsorbate dynamics at metal surfaces, we have chosen pyridine as a more complex adsorbate molecule. Pyridine is a popular anchoring group in molecular electronics where the lowest unoccupied π^* state on gold is less than 1 eV from the Fermi level and, therefore, energetically easily accessible to hot electrons.[16,17] This charge injection barrier can be tuned by attaching different tail groups to pyridine[18] as well as by different binding geometries.[19] The vibrational and electronic properties of pyridine adsorbed on Cu(110) are well known.[16,20–22]

An important ingredient in lowering the charge injection barrier is the large static dipole moment of pyridine.[19,23] The gas phase value of 2.15 D is substantial due to the lone pair on nitrogen.[24] The dipole moment is strongly increased on adsorption to metal surfaces and leads to very large reductions in the work function by typically 2–3 eV.[18,25–31] We recently showed from work function measurements that the dipole moment of pyridine adsorbed on Cu(110) at very low coverages is 6.5 D, decreasing to around 2.5 D at higher coverages.[32] As the work function decreases to a minimum of 1.6 eV,

we observed an enhancement of the nonresonant sum-frequency signal of the surface electrons.[32] From these work function measurements, we deduced that the electric field E_{DC} acting on a single pyridine molecule has a value of $E_{DC} \approx 10^9$ V m^{-1} for a surface density of $n = 4.34 \times 10^{18}$ m^{-2} (1 ML of pyridine). This large field arises as the sum over the molecule's own image dipole and the surrounding molecules' dipoles and their image dipoles. Similarly high fields have been observed for other adsorbates such as NO and CO and have a profound influence on an adsorbate arrangement on the surface.[33]

SFG is capable of detecting electric fields at an interface because in the presence of an electric field (E_{DC}), the third order susceptibility can contribute to the second order nonlinear response via the term $\chi^{(3)}E_{DC}$.[34–38] Detection of the electric field at the interface has been used to monitor potential-dependent effects at electrode surfaces,[39,40] such as difference in adsorbate binding and orientation.[41] At charged aqueous interfaces, the electric field leads to an ordering of water molecules in the electric double layer which can extend the probing depth of SFG beyond the interfacial layer.[34,35,42–46] It has been shown for thick adsorbed proteins layers that the variations on the local optical field might also affect the signal, and third-order effects must be taken into account.[47] In particular, for interfacial water, electric fields have been shown to have an effect on the vibrational dynamics.[48,49]

In our previous work,[32] we used broadband sum and difference frequency generation (DFG) to uncover that photons can be used to manipulate the pyridine work function. The key observations we made are summarized in Fig. 1. Pyridine adsorption reduces the surface work function from 4.5 eV to 1.6 eV. In the ground state of the pyridine adsorbate, its static dipole is determined by the nitrogen lone pair. This binds to the copper surface, and thus, the pyridine dipole is opposed to the surface dipole and lowers the work function. The vibrationally nonresonant sum frequency signal, generated by 1.55 eV and 0.38 eV photons in and 1.93 eV out, increases more than three-fold on adsorption. Switching the upconversion pulse to 2.33 eV and changing to a DFG process so that 2.33 eV – 0.38 eV

= 1.95 eV, i.e., only changing one photon energy, reduces the vibrationally nonresonant difference frequency signal to 15%. Using the same 2.33 eV pulse, as a pump can, in turn, also reduce the SFG. For temporal overlap with the sum frequency pulses, the 2.33 eV pump reduces the bare Cu(110) nonresonant SFG by 7% and the nonresonant SFG of pyridine-covered Cu(110) by 50%, as shown in Fig. 1.

We discussed in our previous work[32] that the most likely explanation for these various observations was a $\chi^{(3)}E_{DC}$ contribution to the copper sum frequency response. E_{DC} is generated by the pyridine layer collective dipole which explains the increase in SFG on adsorption via $\chi^{(3)}E_{DC}$. The 2.33 eV beam is intense enough to cause transfer into the pyridine π^* LUMO. This, much like in the gas phase,[50] reverses the dipole direction in the excited pyridine adsorbates, which leads to a pyridine dipole reversal and, thus, a temporary reduction in the work function and E_{DC}. This explains both the decrease in pumped SFG and also in the DFG process because the 2.33 eV photon reduces E_{DC} of the pyridine adlayer.

In this work, we present a more in-depth analysis of the pyridine ultrafast dynamics following 2.33 eV excitation, where we relate the sum frequency transients to a changing structure of the pyridine adlayer, as revealed by a change in the relative phase between nonresonant copper and resonant pyridine C–H stretching sum frequency signals. The ensuing structural change in the pyridine adlayer lasts for tens of picoseconds. A comparison with transients generated by 1.55 eV shows that electron transfer into the pyridine LUMO occurs from a hot electron bath.

EXPERIMENTAL

Pump sum-frequency generation-probe UHV-spectrometer

We used a chirped-pulse amplifier (Spectra-Physics, TSA-10) to generate femtosecond laser pulses at 10 Hz repetition rate, 150 fs pulse width, and 6 mJ per pulse. The output beam is split into three laser paths: visible (VIS), infrared (IR), and pump. The IR and pump branches (2.2 mJ each) are used for pumping two Travelling-wave Optical Parametric Amplifier of Superfluorescence (TOPAS Light Conversion). In one TOPAS, the signal and idler beams produce in a second stage by noncollinear difference frequency generation in a AgGaS$_2$ crystal tuneable mid-IR (2.8 μm–10 μm). In the other TOPAS, tunable visible pump light is produced via second harmonic generation in a variety of nonlinear crystals. Typical bandwidth is 150 cm^{-1}. The VIS branch is spectrally narrowed by an etalon (SLS Optics Ltd., 7.2 cm^{-1} spectral width) to produce a time-asymmetric pulse or by a home-built pulse-shaper which produced a Gaussian pulse with 5.3 cm^{-1} spectral width.

For the pump-SFG setup, the IR, VIS, and pump beams were overlapped in space and time on the Cu(110) crystal at 65°, 60°, and 63° incidence angles from the copper surface normal, respectively. Beams were incident in between [001] and [1−10] directions, and a low energy electron diffraction (LEED) pattern is shown in the supplementary material (Fig. S1). A single planoconvex CaF$_2$ lens (f′ = +250 mm) was used to focus all the beams, entering the ultra-high vacuum (UHV) chamber through a CaF$_2$ window. For more specific details about beam alignment into the UHV chamber using
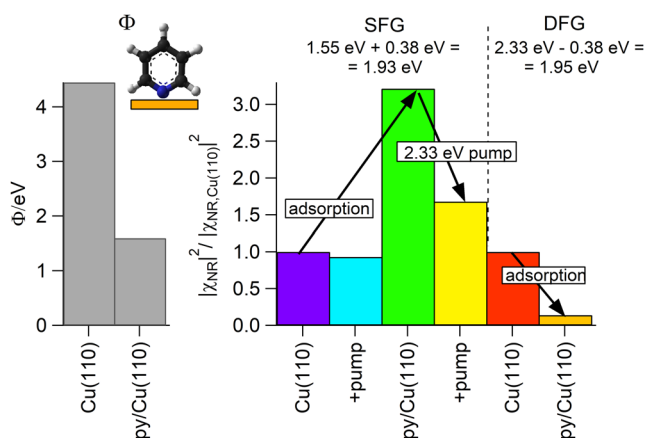

FIG. 1. Left: Work functions for clean Cu(110) and 1 ML pyridine on Cu(110). Right: Summary of the effects of pyridine adsorption and effect of a 2.33 eV pump pulse on sum and difference frequency signals (values taken from Ref. 32).

a "dummy" alignment path outside the UHV chamber; see Arnolds *et al.*[41] The VIS and the pump beam had their focal points after reflecting off the sample to produce larger spot sizes than the IR, which is focused on the sample. A telescope was inserted in the VIS path to vary the 800 nm spot size. The beam diameters (full width half maximum) are approximately 350, 300, and 150 μm at the sample position, for the pump, VIS, and IR, respectively. For detection, we used a 0.3 m spectrograph (Acton SpectraPro 300i) and intensified charge-coupled device (ICCD) (Andor iStar). For one spectrum, typically the signal from 1000 to 2000 shots was accumulated with full 0.7 cm^{-1}/pixel resolution. The UHV-SFG spectrometer layout is presented in the supplementary material (Fig. S2).

Spatial and temporal overlap of all three beams is first achieved outside the chamber using a pinhole and a 1 mm thick LiIO$_3$ crystal. Spatial overlap inside the chamber between pump and VIS pulse is initially monitored by a camera. The sum-frequency signal at 646 nm on a clean Cu(110) crystal is first optimized by moving the VIS beam in space and time. The Cu(110) crystal is then rotated slightly to detect the pump-IR difference-frequency signal at 635 nm, which is optimized by adjusting the pump beam only. The Cu(110) crystal is then rotated back toward the sum frequency position, overlap with the VIS beam is checked, and the time delay adjusted. Final overlap with a green pump pulse can be optimized by noticing the reduction in the bare copper nonresonant background (Fig. S6) and a reduced intensity of the copper sum frequency spectrum at lower wavelengths and higher frequencies (see Fig. S7).

The time delay for pump-probe transients is the delay between arrival of the pump pulse and arrival of the visible upconversion pulse. For Gaussian upconversion pulses produced with a pulse shaper, the infrared pulse intensity maximum coincides in time with the upconversion pulse maximum. To probe changes in height and frequency more accurately,[51] we also used a time-asymmetric pulse shaped by an etalon. The etalon-shaped pulse either coincides with the IR pulse to record the nonresonant background plus the molecular resonance or is time-shifted by 600 fs to record just the resonance. For pump-probe studies with an etalon-shaped upconversion pulse, the time delay is still defined as the delay between pump and the visible probe pulse as that is the point at which we start to generate the sum frequency signal; see the supplementary material, Fig S3, for an illustration.

Typical incident 2.33 eV pump pulse energy was 120 μJ. The cross correlation between the IR-VIS pulses shows a time resolution of 400 fs for the nonresonant-SFG signal. The time resolution of the resonant SFG signal is determined by the pyridine C–H vibrational dephasing time, which is around 2 ps for our 5 cm^{-1} linewidth.

UHV techniques and sample preparation

Pump-probe sum frequency generation measurements were carried out in an ultra-high vacuum (UHV) chamber at a base pressure of 3×10^{-10} mbar and crystal base temperature of 100 K. The Cu(110) crystal was cleaned by repeated cycles of 500 V Ar$^+$ ion sputtering and 650 K annealing until a sharp LEED (1 × 1) pattern was obtained. The sample cleanliness was confirmed by reproducible sum frequency spectra and temperature programmed desorption (TPD) at 2 K s^{-1} recorded with a quadrupole mass spectrometer (MKS Microvision-2).

Pyridine (anhydrous, 99.8%, SigmaAldrich) was dosed from the liquid after several freeze-pump-thaw cycles, through a 20 cm long stainless-steel tube to provide a degree of directional dosing. Different surface coverages were prepared by annealing to different temperatures. Dosing about one monolayer at 100 K typically took 20 min at an m/z 52 partial pressure of around 10^{-10} mbar.[32] The m/z 52 corresponds to the fragmentation of pyridine molecular ions to form $[C_4H_4]^{+\cdot}$, formed in higher numbers than the parent ion at m/z 79. Coverage can be calibrated by temperature-programmed desorption (TPD). We define here as 1 ML the coverage obtained by dosing a slight multilayer of pyridine (sharp desorption peak at 151 K) and briefly heating the crystal to 200 K. This preparation generates the largest sum frequency signal and a work function of about 1.7 eV.[32]

RESULTS AND DISCUSSION

Pump-probe spectroscopy of pyridine

Adsorbed pyridine possesses a single vibrational mode in the C–H stretching region, which we assigned to the ν_2 vibration, where all C–H bonds vibrate in phase. Pyridine has two other allowed totally symmetric modes, ν_{20a} and ν_{13}, but these have much smaller predicted infrared and Raman intensities.[32]

Figure 2 shows pyridine sum frequency spectra without pump and with 2.33 eV pump at 0 and 5 ps delay from the sum frequency probe pulses. The spectra consist of the spectrally broad sum frequency response of the surface electrons (the nonresonant background) and the pyridine C–H resonance for a Gaussian upconversion pulse. The spectra are not normalized with respect to the incoming IR intensity; instead, the IR envelope (obtained from a smoothed sum frequency spectrum of bare copper) is shown. As shown previously and summarized in Fig. 1, the nonresonant background drops at short delay times but recovers for longer delays. In addition, the spectra show a decreasing height of the resonance and a changing shape with respect to the nonresonant background.
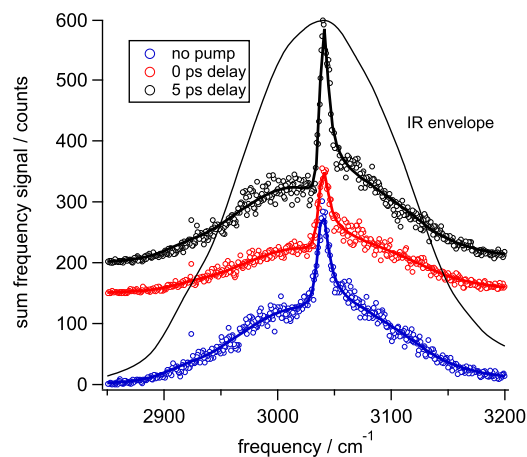
FIG. 2. Pyridine sum frequency spectra with and without 532 nm pump pulse at different time delays (incident pulse energy 122 μJ). Pyridine was dosed to a slight multilayer and briefly annealed to 200 K, spectra acquired at 100 K as a coaddition over 2000 laser pulses. The IR envelope was obtained from a bare copper sum frequency spectrum. A Gaussian upconversion pulse was used.

The shape change is due to a phase difference between the sum frequency emitted by surface electrons and by the molecule, which leads to changes in how the two signals interfere. The total spectrum can be described by the standard equation[52]

$$I_{SFG} \approx \left| \chi_{NR}^{(2)} + \chi_{RES}^{(2)} \right|^2 = \left| A_{NR} e^{i\varphi} + \frac{A_{RES}}{(\omega_{IR} - \omega_{RES}) + i\Gamma_{RES}} \right|^2, \quad (1)$$

where A_{NR} is the height of the nonresonant background, φ is the relative phase between nonresonant and vibrationally resonant responses, A_{RES}, ω_{RES}, and Γ_{RES} are the Lorentzian amplitude, center frequency, and width, respectively, and ω_{IR} is the incoming IR frequency. To fit spectra like those shown in Fig. 2, this expression is multiplied by the IR envelope.

Fitting a sum frequency intensity spectrum possesses two solutions for a single resonance, which differ in the relative phase and height of the resonance.[53] When we previously studied the pyridine coverage dependence,[32] the two solutions differed by the size of the phase change during pyridine adsorption. We discounted the solution with the larger phase change because there was no discernible chemical reason for seeing large phase changes for relatively high coverages, when little changes on the surface. For these pumped spectra, we similarly find a solution with a large phase change as a function of time delay but discount it because the corresponding resonant height increases in the transient. Given that spectra recorded with a time-shifted time-asymmetric visible upconversion pulse clearly show that the resonant height decreases, we can discount this solution (examples of these spectra are shown in Fig. S4, and C–H height transients obtained from resonant + nonresonant and resonant only spectra are shown in Fig. S5). The second solution with the overall smaller phase change is plotted in Fig. 3 and shows that the relative phase φ between resonant and nonresonant sum frequency contributions changes by up to 20°.

The height transients in Fig. 3 show the same phenomenon as reported previously[32] for time delays up to 10 ps. The nonresonant sum frequency signal of the pyridine-covered surface is reduced for short delay times. As indicated in Fig. 1, the bare copper surface signal under these conditions changes by less than 10%. Alongside the coverage-dependent changes in sum and difference frequency signals, this dip allowed us to show[32] that the second-order polarizability of a pyridine-covered surface $P^{(2)}$ contains contributions from both a second-order susceptibility $\chi^{(2)}$ and a third-order susceptibility $\chi^{(3)}$ in combination with a static field E_{DC}

$$P^{(2)}(\omega = \omega_1 \pm \omega_2) = \left(\chi^{(2)} + \chi^{(3)} E_{DC} \right) E(\omega_1) E(\omega_2). \quad (2)$$

E_{DC} for an individual pyridine molecule is given by the sum over its own image dipole and the dipoles and image dipoles of the surrounding pyridines and has a value of approximately 10^9 Vm^{-1} as explained previously.[32] The 2.33 eV pump pulse can excite electrons into the pyridine LUMO, which reverses the pyridine dipole and reduces E_{DC}. The nonresonant signal is reduced for a relatively long time, with a time constant of approximately 460 fs, which we suggested could be due to a stabilization of the reversed dipole of an excited pyridine by neighboring ground state pyridines.[32,33]

Expanding on our previous work,[32] we now look into the transient changes in the C–H resonance in more detail. The resonant C–H stretch sum frequency signal shows a subpicosecond as well as a much slower response. Only the size of the signal changes, while changes in the frequency and width of the C–H resonance are minimal as seen in Fig. 3. This might appear surprising in comparison with the well-studied cases of CO on various metal surfaces, but the likely reason is that the C–H stretching mode is well decoupled from changes to the pyridine π system and changes in surface charge distribution.[54] Even the C=C ring stretching mode only exhibited a Stark shift of 6 cm^{-1} for an applied field of $\approx 3 \times 10^9$ V m^{-1},[55] and
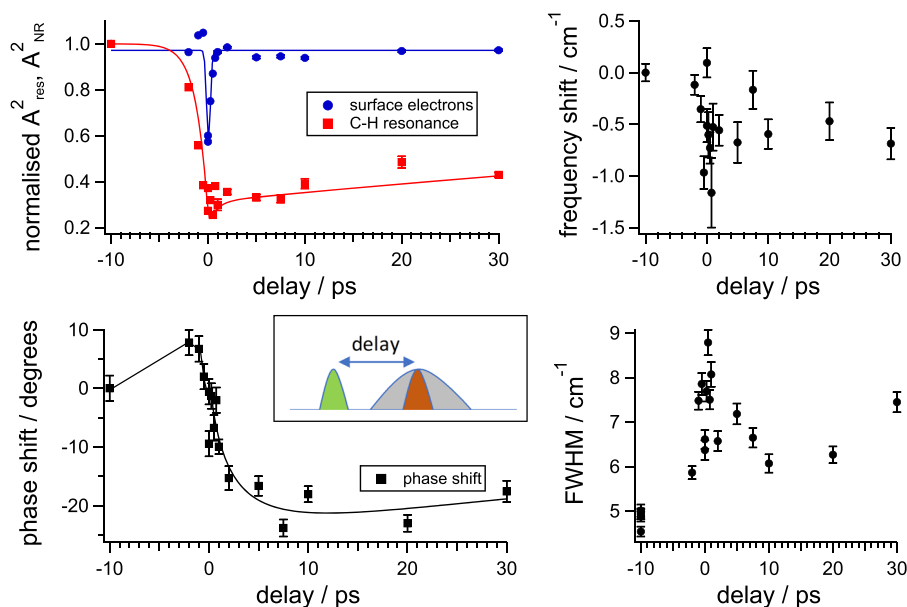

FIG. 3. Pump (2.33 eV) – sum frequency probe transients for a 200 K annealed pyridine layer on Cu(110), recorded at 100 K. Top left: nonresonant and resonant sum frequency peak heights (A_{NR}^2 for surface electrons and A_{Res}^2 for C–H stretch, respectively). Solid lines are fits to the data as explained in the text. Bottom left: their relative phase φ. Frequency shift and changes in resonant width are shown on the right. All points are normalized to their unpumped values, here placed at 10 ps.

our pump-induced changes in field must be smaller than the ground state adsorbate field of 10^9 V m^{-1}.

The C–H transient in Fig. 3 possesses a subpicosecond dip with a more gradual onset at negative time delays than the nonresonant transient. The pump pulse perturbs the free induction decay of the resonance, which has a dephasing time of 2.1 ps deduced from a line width of 5 cm^{-1}. Probing dynamics with a vibrational resonance reduces the time resolution of the experiment compared to the instantaneous response of the surface electrons to the probe pulses.

Given the temporal coincidence between the initial reduction in the C–H sum frequency signal and the reduction in the nonresonant surface electron signal, we propose that a significant part of the resonant response must be due to a $\chi^{(3)} E_{DC}$ term, just as for the nonresonant response.

We can estimate the sizes of $\chi^{(2)}$ and $\chi^{(3)}$ for the pyridine C–H stretch, following Wang *et al.*[47] We detect the pyridine ν_2 C–H stretching mode, which involves the C2, C4, and C5 carbons with a net dipole moment change along the C$_{2v}$ axis of 0.49 D/Å. Since this is a symmetric stretch involving three hydrogens, we can use the following expression for the molecular hyperpolarizability

$$\beta^{(2)}_{ccc} = -\frac{1}{2\varepsilon_0 \omega_0} \frac{\partial \alpha}{\partial Q} \frac{\partial \mu}{\partial Q} = -\frac{1}{2\varepsilon_0 \omega_0} \frac{3}{m_H} \frac{\partial \alpha}{\partial r} \frac{\partial \mu}{\partial r}, \quad (3)$$

where Q is the normal mode and r is the C–H bond coordinate.

Using $\partial\alpha/\partial r = 3 \times 10^{-30}$ C m V^{-1}, we obtain $\beta^{(2)}_{ccc} = 8.5 \times 10^{-27}$ m^4 V^{-1} and for our monolayer density of 4.3×10^{18} m^{-2}, this results in

$$\chi^{(2)}_{zzz} = 2.4 \times 10^{-20} \text{ m}^2 \text{ V}^{-1}.$$

We can similarly estimate the third-order susceptibility using the values given by Wang *et al.* and obtain $\chi^{(3)}_{zzzz} = 1.26 \times 10^{-29}$ m^3 V^{-2}. For an electric field of 10^9 V m^{-1}, we obtain

$$\chi^{(3)}_{zzzz} = E_{DC}/\chi^{(2)}_{zzz} = 0.5.$$

This estimate shows that the third-order contribution can be substantial for our C–H resonance for a high pyridine coverage. While we have no means of estimating the susceptibilities for the excited state of adsorbed pyridine, the estimate above shows that our explanation is compatible with known susceptibilities for C–H stretches. In addition, the temporal coincidence between the fast dips in nonresonant and resonant signals lends support to our interpretation that the initial decay of the C–H signal is due to the field reversal.

The slow recovery of the C–H signal over the range of tens of picoseconds cannot be explained by an electric field effect, but we note from Fig. 3 that the relative phase between nonresonant and resonant signals recovers on a similar time scale. The change in relative phase φ can have its origin in the substrate phase, the adsorbate phase, or both. It is not clear *a priori* that the phase of the copper sum frequency response remains constant on excitation by the pump pulse since the pump pulse excites copper electrons. We have been unable to measure the absolute phase of the copper sum frequency signal, but we can at least estimate the time scale over which the metal phase might evolve independently from the

adsorbate phase from the bare copper response to the pump pulse. As shown previously,[32] the bare copper sum frequency signal is reduced by a small amount, which could potentially be due to a small temperature dependence of $\chi^{(2)}$.[56,57] This reduction only lasts for about 600 fs (data shown in Fig. S6 in the supplementary material), which is much faster than any changes seen in the phase in Fig. 3. We also noticed that around zero time delay, the nonresonant sum frequency spectrum of copper is reduced at the high frequency edge (see Fig. S7). This phenomenon disappears within about 200 fs and could be caused by the pump pulse changing the electron distribution of the copper substrate. Based on the short-lived pump-induced effects on the copper substrate sum frequency spectra, we consider that the long-lived relative phase change in Fig. 3 is not caused by optical excitation of the metal surface and turn to other explanations.

Relative phase shifts between nonresonant and resonant sum frequency signals have been seen frequently. For example, oxidation of a surface leads to phase shifts of close to 180°,[13,19] while changes in electrode potential change the relative phase between 4-cyanopyridine and various noble metal alloy surfaces by around 30°–40°.[58] These changes are commonly attributed to a change in the electronic structure of the adsorbate-substrate system. We equally suggest that the observed phase change indicates a change in the electronic structure of adsorbed pyridine, which leads to a different phase and an overall smaller nonlinear susceptibility.

Given that the sum frequency amplitude remains low for tens of picoseconds while the pyridine phase is changed, one possibility would be for the pyridine molecule to tilt so that the effective surface normal component of the C–H dynamic dipole moment is reduced. This would, however, at the same time reduce the effective normal component of the pyridine static dipole, which would lower E_{DC}. We consider this scenario unlikely because at delay times longer than about 2 ps, the surface electron signal has fully recovered while the C–H signal is still much reduced.

We propose instead an in-plane rotation of the pyridine with a schematic sketched in Fig. 4. The effect of the pump pulse is to excite electrons into the pyridine LUMO, most likely by creating a hot electron distribution, as discussed later. This excitation creates anions within a neutral adsorbate layer. Surrounding neutral pyridines could minimize their interaction with the pyridine anion by rotating their π electron clouds away from the anion such that the more positive hydrogen atoms point toward it. The ensuing structural changes carry on beyond the lifetime of the reversed dipole (ca 460 fs), leading to an adsorbate layer with now unfavorably oriented pyridines with respect to the copper in-plane directions. This "disorder" needs tens of picoseconds to relax back to a pyridine layer with a good in-plane order.

The bonding of pyridine to the copper surface involves both a σ bond and a π bond of the nitrogen lone pair with the copper d-orbitals. Atodiresei *et al.* showed that a relatively large barrier of 0.4 eV (caused by the π bond) normally hinders the rotation of an individual pyridine molecule from the [001] to the [1–10] direction.[59] If the electrostatic interaction with a pyridine anion can overcome this barrier, then any pyridine which rotates as a result will not be able to easily rotate back because the available thermal energy is low. A rotation would reduce overlap with the copper d-orbitals, which in turn means a lower electron density on the molecule and thus a lower nonlinear susceptibility.
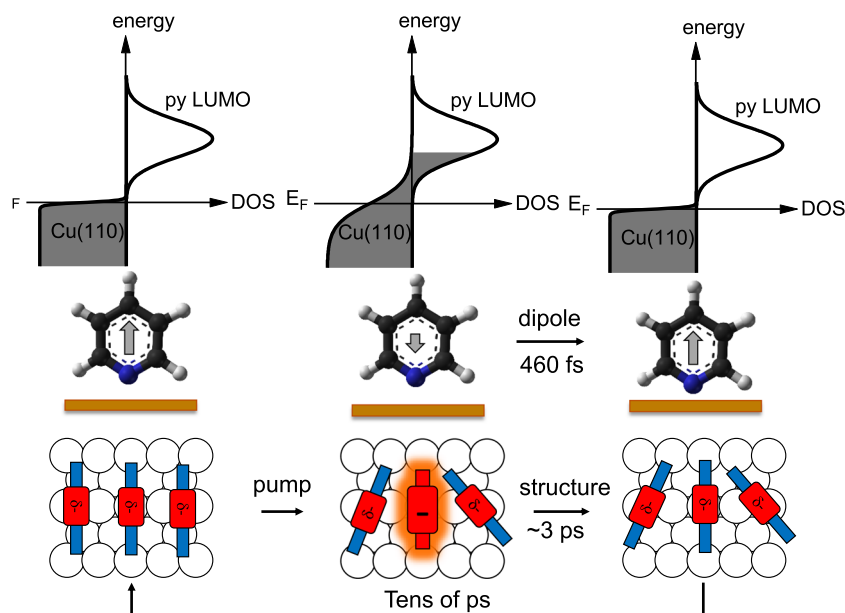
FIG. 4. Illustration of the model to explain the observed dynamics. The femtosecond pump pulse produces a hot electron distribution, which populates the pyridine π^* states and reverses the adsorbate dipole on a time scale of 460 fs. The molecules neighboring the anion reorient to minimize interaction with the negative charge, and a new structure is created on a time scale of 3 ps. The new orientation finally relaxes within tens of ps.

The transients we see in Fig. 3 are broadly compatible with this model. Using the time scales seen in the nonresonant background and in the phase, we can model the resonant height changes by a set of coupled differential equations (see the supplementary material for details). Briefly, we consider the C–H height to be representative of the pyridine ground state which is depleted by pump-induced generation of an anion with a lifetime of 460 fs. This lifetime is derived from the dip of the nonresonant sum frequency signal.[32] The presence of the anion in the layer leads to the generation of an intermediate state where the two nearest neighbor pyridines rotate within the copper plane, which finally relaxes back to the ground state. The resulting traces are then convoluted with the lifetime of the C–H stretch of 2.1 ps. As can be seen by the solid line in Fig. 3, the general shape of the C–H transient can be described well by this rough phenomenological model and results in a time constant of around 500 fs for generation of the intermediate state and a thermal relaxation over 170 ps. The shape of the phase transient would then be represented by the population of the twisted state. As the solid line in Fig. 3 shows, the phase is not as well described by these time constants, but that lies probably in the very simplified assumption that only nearest neighbors react to the anion and that presence of rotated pyridines has no further influence on surrounding ground state pyridines.

We test this model by studying the coverage dependence of the pump-probe transients. If the assumptions above are correct, then a lower coverage and, therefore, larger average distance between a pyridine anion and neighboring pyridines will lead to a disappearance of the effect.

Coverage- and wavelength-dependent dynamics

Figure 5 shows pump-probe transients for the C–H stretch on three different layers—as-dosed to approximately 1.3 ML (a work function of 1.7 eV, slightly beyond the minimum work function),

annealed to 200 K, which generates the highest SFG signal (work function also ≈1.7 eV), and annealed to 240 K, which reduces the coverage and increases the work function to 2.1 eV.

When pyridine molecules occupy a second layer, the C–H signal becomes very small, so we recorded all spectra with a time-shifted upconversion pulse to remove the nonresonant background.
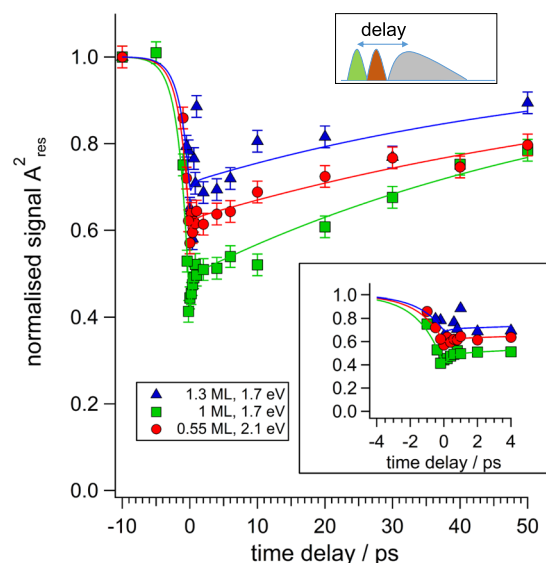

FIG. 5. Pump-probe transients at 100 K for a multilayer as dosed (1.7 eV work function) and subsequently annealed to 200 K (1.7 eV) and 240 K (2.1 eV). Lines are drawn to guide the eye. Incident pulse energy of the pump was 67 μJ. Data were acquired with a time-shifted etalon-shaped upconversion pulse as indicated in the sketch.

See the supplementary material (Fig. S8) for the spectra at different coverage pump-probe delays.

The 200 K annealed layer shows the largest response at short delay times, where we monitor changes in E_{DC} in the layer, and also at long times, where we monitor structural changes in the adlayer.

The field values of E_{DC} for multilayer and 200 K annealed layer are similar because the multilayer coverage is only just beyond the minimum in the work function. The fast effect can be reduced because the second layer of pyridine molecules can depolarize the first layer, which would in turn reduce the effect of the anion on the surrounding layer. In addition, second layer molecules could sterically hinder the rotation of the first layer.

The fast response decreases when we decrease coverage by annealing to 240 K because we are gradually lowering the field, but we are also losing the long-term response. This is sensible for two reasons; with increasing distance from one another, the effect of a pyridine anion on neighboring pyridines is reduced, so less rotation within the surface plane would occur. At the same time, the work function is higher which implies that the LUMO is also further away from the Fermi level and might not be excited as efficiently. If we reduce the coverage even further by annealing to higher temperatures, the effect completely disappears (see the supplementary material, Fig. S8D).

To test whether the pyridine dynamics are caused by nascent or hot electrons, we changed the wavelength of the pump pulse to 800 nm, corresponding to 1.55 eV photon energy. To determine the pump fluence with respect to the 2.33 eV beam, we recorded CO pump-probe spectra in separate experiments. The CO transients on Cu(110) have be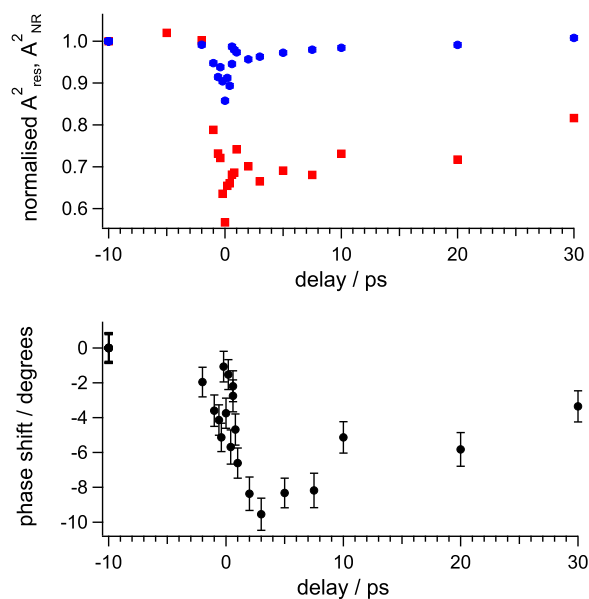en shown to be independent of pump wavelength[14,15] (also see the supplementary material, Fig. S9). From the frequency transients (shown in the supplementary material, Fig. S10), we can estimate that the fluence was ca 3× smaller than in Fig. 1. The 1.55 eV pump transients of pyridine are shown in Fig. 6.

Even though the fluence is significantly smaller, we can still clearly discern the fast changes in nonresonant and resonant signals at short pump delays and the phase shift is also still clearly apparent.

A photon energy of 1.55 eV is only able to excite electrons from the copper sp bands, which have a much lower density of states than the copper d band. This means the cross section for any process caused by excitation of nascent electrons is much reduced for photon energies below 2 eV.[60] Since the effects scale roughly with absorbed fluences as measured by CO transients, we suggest that the effects seen are caused by hot electrons tunneling into the pyridine LUMO.

From the point of view of manipulating the surface-work function by photon excitation, the ensuing changes in the adsorbate layer observed here are a drawback. However, pyridine has been linked to gold surfaces via an araliphatic backbone which improves order and stability of the layer,[54,55] which might be a way forward to isolate the subpicosecond response seen here.

CONCLUSIONS

We have shown that the sum frequency resonance of pyridine on copper in vacuum is enhanced by a $\chi^{(3)}$ contribution due to the substantial static electric field generated by the pyridine adsorbate layer. The previously investigated field reversal caused by a pump pulse leads at long delay times to a substantially reduced resonant response. This is characterized by a different relative phase and can be rationalized by a weaker molecule-surface bond potentially caused by the in-plane rotation.

SUPPLEMENTARY MATERIAL

See supplementary material for details on the Cu(110) crystal orientation and the ultra-high-vacuum sum frequency generation spectrometer, the definition of the time delay and pump-probe transients recorded with an etalon-shaped pulse, pump-probe measurements on bare Cu(110), pump-probe measurements on CO adsorbed on Cu(110), which was used as a thermometer to estimate the pump-induced heating, and the description of the differential equation fitting for the pump-probe measurements to extract the pump-induced dynamics on the pyridine adsorption on Cu(110).

FIG. 6. Pump (1.55 eV)—sum frequency probe transients for a 200 K annealed pyridine layer on Cu(110), recorded at 100 K. Incident pulse energy of the pump was 310 μJ. Top: nonresonant and resonant sum frequency peak heights (A_{NR}^2 for surface electrons and A_{Res}^2 for C–H stretch, respectively). Bottom: their relative phase φ. All points are normalized to their unpumped values, here placed at 10 ps.

REFERENCES

[1] M. Galperin et al., Science **319**, 1056 (2008).
[2] W. Ni et al., Nano Lett. **10**, 77 (2010).
[3] P. Hu et al., J. Phys. Chem. Lett. **9**, 5167 (2018).
[4] A. Vilan, D. Aswal, and D. Cahen, Chem. Rev. **117**, 4248 (2017).
[5] J. C. Tully, Annu. Rev. Phys. Chem. **51**, 153 (2000).

[6]H. Arnolds and M. Bonn, Surf. Sci. Rep. **65**, 45 (2010).

[7]E. H. Backus et al., Science **310**, 1790 (2005).

[8]M. Bonn et al., Phys. Rev. Lett. **84**, 4653 (2000).

[9]K.-I. Inoue, K. Watanabe, and Y. Matsumoto, J. Chem. Phys. **137**, 024704 (2012).

[10]B. L. Maschhoff and J. P. Cowin, J. Chem. Phys. **101**, 8138 (1994).

[11]M. Bonn et al., Science **285**, 1042 (1999).

[12]I. M. Lane et al., Phys. Rev. Lett. **97**, 186105 (2006).

[13]D. Novko, M. Alducin, and J. I. Juaristi, Phys. Rev. Lett. **120**, 156804 (2018).

[14]T. Omiya and H. Arnolds, J. Chem. Phys. **141**, 214705 (2014).

[15]T. Omiya et al., Surfaces **2**, 117 (2019).

[16]D. B. Dougherty, J. Lee, and J. T. Yates, Jr., J. Phys. Chem. B **110**, 11991 (2006).

[17]D.-Y. Wu et al., J. Phys. Chem. C **112**, 4195 (2008).

[18]Z. Ma et al., Phys. Chem. Chem. Phys. **13**, 9747 (2011).

[19]M. Kamenetska et al., J. Am. Chem. Soc. **132**, 6817 (2010).

[20]S. Haq and D. A. King, J. Phys. Chem. **100**, 16957 (1996).

[21]J. G. Lee, J. Ahner, and J. T. Yates, J. Chem. Phys. **114**, 1414 (2001).

[22]T. Gießel et al., J. Chem. Phys. **110**, 9666 (1999).

[23]Y. Ie et al., J. Am. Chem. Soc. **133**, 3014 (2011).

[24]B. B. Demore, W. S. Wilcox, and J. H. Goldstein, J. Chem. Phys. **22**, 876 (1954).

[25]J. L. Gland and G. A. Somorjai, Surf. Sci. **38**, 157 (1973).

[26]D. Heskett et al., Surf. Sci. **197**, 225 (1988).

[27]Q. Zhong, C. Gahl, and M. Wolf, Surf. Sci. **496**, 21 (2002).

[28]J. E. Whitten, Surf. Science **546**, 107 (2003).

[29]G. Heimel et al., Nano Lett. **7**, 932 (2007).

[30]S. Bahr and V. Kempter, J. Chem. Phys. **127**, 174514 (2007).

[31]O. T. Hofmann et al., J. Chem. Phys. **139**, 174701 (2013).

[32]N. García Rey et al., J. Phys. Chem. C **121**, 6692 (2017).

[33]P. Deshlahra et al., Langmuir **28**, 8408 (2012).

[34]S. Ong, X. Zhao, and K. B. Eisenthal, Chem. Phys. Lett. **191**, 327 (1992).

[35]Y.-C. Wen et al., Phys. Rev. Lett. **116**, 016101 (2016).

[36]G. Gonella et al., J. Phys. Chem. C **120**, 9165 (2016).

[37]E. Tyrode and R. Corkery, J. Phys. Chem. C **122**, 28775 (2018).

[38]N. García Rey et al., J. Phys. Chem. C **123**, 1279 (2019).

[39]P. Koelsch et al., J. Opt. Soc. Am. B **30**, 219 (2013).

[40]N. García Rey and D. D. Dlott, J. Electroanal. Chem. **800**, 114 (2017).

[41]H. Arnolds et al., Rev. Sci. Instrum. **74**, 3943 (2003).

[42]X. Zhao, S. Ong, and K. B. Eisenthal, Chem. Phys. Lett. **202**, 513 (1993).

[43]K. B. Eisenthal, Chem. Rev. **96**, 1343 (1996).

[44]F. M. Geiger, Annu. Rev. Phys. Chem. **60**, 61 (2009).

[45]A. G. F. d. Beer, R. K. Campen, and S. Roke, Phys. Rev. B **82**, 235431 (2010).

[46]K. C. Jena, P. A. Covert, and D. K. Hore, J. Phys. Chem. Lett. **2**, 1056 (2011).

[47]J. Wang et al., J. Phys. Chem. B **108**, 3625 (2004).

[48]A. Eftekhari-Bafrooei and E. Borguet, J. Am. Chem. Soc. **131**, 12034 (2009).

[49]A. Eftekhari-Bafrooei and E. Borguet, J. Phys. Chem. Lett. **2**, 1353 (2011).

[50]R. M. Hochstrasser and J. W. Michaluk, J. Chem. Phys. **55**, 4668 (1971).

[51]A. Lagutchev, S. A. Hambir, and D. D. Dlott, J. Phys. Chem. C **111**, 13645 (2007).

[52]A. G. Lambert, P. B. Davies, and D. J. Neivandt, Appl. Spectrosc. Rev. **40**, 103 (2005).

[53]B. Busson and A. Tadjeddine, J. Phys. Chem. C **113**, 21895 (2009).

[54]A. T. Zayak et al., Phys. Rev. Lett. **106**, 083003 (2011).

[55]Y. Ikezawa et al., Electrochim. Acta **43**, 3297 (1998).

[56]J. Hohlfeld et al., Appl. Phys. A **60**, 137 (1995).

[57]J. Hohlfeld, U. Conrad, and E. Matthias, Appl. Phys. B **63**, 541 (1996).

[58]K. H. Frank, R. Dudde, and E. E. Koch, Chem. Phys. Lett. **132**, 83 (1986).

[59]N. Atodiresei et al., Phys. Rev. B **78**, 045411 (2008).

[60]N. García Rey and H. Arnolds, J. Chem. Phys. **135**, 224708 (2011).